Proceedings of the Korean Nuclear Spring Meeting
Gyeong ju, Korea, May 2003

In-situ Raman Spectroscopic Study of Oxide Films on Alloy 600 in Simulated PWR Water

Ji Hyun Kim and Il Soon Hwang

Seoul National University
56-1, Shinlim-dong, Gwanak-ku
Seoul, Korea 151-742

Abstract

Although there has been no general agreement on the mechanism of intergranular stress corrosion cracking (IGSCC) as one of major degradation modes of Ni-base alloys in PWR's, common belief derived from previous studies is that the damage to the alloy substrate is related to mass transport characteristics and/or repair properties of overlaying oxide film. Recently, it was shown that the oxide film structure and IGSCC initiation time aw well as crack growth rate were systematically varied as a function of hydrogen partial pressure in high temperature water, providing supporting evidences. This study is aimed at demonstrating a capacity to characterize the oxide film by an in-situ Raman spectroscopy as a function of PWR primary water conditions in order to understand how the oxide film chemistry can vary with water chemistry and participate in the cracking process as a key variable. This is achieved by analyzing the oxide film properties obtained for alloy 600 in various conditions leading to different IGSCC susceptibility. The in-situ Raman spectroscopic information obtained for various oxide films on alloy 600 in primary water of PWR as a function of hydrogen partial pressure is compared with thermodynamic predictions.

1. Introduction

Primary water stress corrosion cracking (PWSCC) is one of major degradation modes that have been observed to occur pre-dominantly along grain boundaries in Ni-base structural materials for steam generators (SG's) or nozzles in the primary circuit of nuclear power plants. Such an intergranular stress corrosion cracking (IGSCC) has been observed under specific combinations of materials and environmental conditions.[1] The PWSCC of alloy 600 is directly related with safety concerns of nuclear power plant from the viewpoint that the SG tubings or nozzles may rupture as result of the cracking although alloy 600 components are protected against rupture by relatively large safety margins. Also, it has been intensified in recent years as Ni-base alloys display the increasing number of IGSCC events in components

that are critical to the life extension of nuclear power plants.

The PWSCC phenomenon of alloy 600 has been extensively studied in order to formulate remedies and to establish theoretical and/or empirical models for predicting the crack initiation time and crack growth rates for field components.[2-7] Several theoretical and semi-empirical models, based on slip dissolution/ oxidation[2], corrosion-enhanced plasticity[3], internal oxidation[4,5] and creep[6,7] have been proposed. Even though there is no general agreement on the mechanism of IGSCC, one common postulation from these studies is that the damage to the alloy substrate can be related to mass transport characteristics, rupture and/or repair properties of overlaying oxide film.

Earlier studies have shown that dissolved hydrogen concentration in high temperature water affects the PWSCC susceptibility of nickel base alloys.[3,8-9] Test results have demonstrated that the maximum of crack growth rate, with respect to dissolved hydrogen concentration variation, is observed in proximity to a key phase transition between the nickel metal (Ni) and nickel oxide (NiO). Fig. 1 summarizes Influence of hydrogen concentration on the crack growth rate of PWSCC in alloy 600 at 360°C.[10] As shown in Fig. 1, the region of degradation by PWSCC is located at transition of nickel metal (Ni) to nickel oxide (NiO) phase. Recently, it was also shown that the oxide film structure, PWSCC initiation time and crack growth rate were systematically varied as a function of hydrogen partial pressure in high temperature water.[10-12] These are evidences that the oxide film on the surface of alloy 600 in the primary water plays a key role in the process of PWSCC.

This study is aimed at characterizing the oxide film by in-situ Raman spectroscopy under PWR primary water conditions in order to understand how the oxide film behaves in the cracking process as a key element. This can be done by analyzing oxide film properties obtained in various conditions exhibiting different PWSCC susceptibility. The in-situ Raman spectroscopic information is to be acquired in this study from the oxide film of alloy 600 metal surfaces in simulated PWR primary water conditions through a hermetically sealed window. The system developed in this study is capable of examining the effect of temperature, dissolved hydrogen concentration, and impurity concentration on chemistry and kinetics of film formation at temperature of up to 350°C and pressure of up to 18 Mpa. On the theoretical side, thermo-chemical calculation has been made to identify the thermodynamically stable oxide phases and to compare with observed results in this work.

2. Experimental

2.1. Materials

The alloy 600 used in this work for analysis of the oxide films have been produced by Sumitomo Metals, Inc., for International Cooperative Group of Environmentally Assisted Cracking (ICG-EAC) round robin test program following the specification of a reactor pressure vessel (RPV) head penetration materials for control rod drive mechanisms (CRDMs) in PWRs.

Chemical composition of alloy 600 used in this study is given in Table 1. The material was solution-annealed at 1050°C for 2 hours and then water-cooled.

The microstructure showed particularly solutionized carbides with an average grain size of

about 50 μm.

2.2. Specimens for Raman Spectroscopic Measurement

The in-situ Raman specimen for aqueous corrosion was machined of alloy 600 into a round disk with 7 mm diameter and 1 mm thickness. All the specimens were mechanically polished down to 1μm Al_2O_3 powder, then rinsed with ethanol, and finally with deionized water prior to an installation for exposure.

For measurements of ex-situ spectra in the air, the commercial high purity powders (Johnson Matthey) of NiO (99.998%), $NiFe_2O_4$ (99%), Cr_2O_3 (99.998%), and $NiCr_2O_4$ (90%) were used to obtain reference spectra for aqueous corrosion of alloy 600. Average particle size was 44μm for NiO, for 200 μm $NiFe_2O_4$, 800μm for Cr_2O_3, and 150μm for $NiCr_2O_4$. Powder color was dark green for NiO, brown for $NiFe_2O_4$, and green for Cr_2O_3 and $NiCr_2O_4$. Powder samples were placed in the recess of sample holder, mixed with deionized water, and then dried prior to deposition on the sample holder.

2.3. Test Conditions

For the surface oxide formation, the alloy 600 specimens were placed inside a high-pressure optical cell and exposed to deionized and deaerated water environments. The same chemical condition as typical PWR primary water was used. Water with a resistivity of 18 MΩ-cm was mixed with additional chemicals to produce 1,000 ppm boron in the form of boric acid(H_3BO_3) and 2 ppm lithium in the form of lithium hydroxide (LiOH).

Two different levels of dissolved hydrogen gas (30 cm^3(STP)/kg or 1 cm^3(STP)/kg) concentration were prepared with corresponding dissolved hydrogen concentrations of 2.68 ppm and 0.89 ppm, respectively, according to the solubility data.[13] The operating pressure was about 18 Mpa and the temperature was varied from room temperature to 350°C.

2.4. Apparatus for In-situ Raman Measurement

The optical cell for the in-situ observation at high temperature and pressure condition was constructed with a custom-designed 1 liter-capacity autoclave. In order to reduce corrosion products from the surfaces of construction materials at high temperature, the cell was made of alloy 690. For the same reason, the head of a water-charging pump was made of titanium and balls of check valves were made of sapphire. All other components exposed to high temperature water including compression fittings and tubings were made of alloy 600. The nominal flow rate to the cell was maintained at 4 liters per hour during experiments. The cell was machined with two penetrations in the wall of cylinder to place optical windows for the access of Raman spectroscopy. The initial window assembly, composed of 4.5 mm thick sapphire with gaskets to seal high-pressure water, was designed after Hurst et al.'s work.[14] In this work, gaskets were made of Ni-base alloy 718 electroplated with gold to 25 μm thickness. Because the optical surface of the sapphire was degraded by pitting corrosion in high

temperature water during the study, a 0.25 mm thick CVD diamond disk was placed on the water side of the sapphire window and this has greatly reduced surface attack on the sapphire window. The alloy 600 specimen for aqueous corrosion was held in the recess of an oxidized zirconium metal by a washer made of alloy 718 with the gasket of an oxidized zirconium sheet so as to electrically insulate the specimen for the cell.

The Raman spectroscopy system is consisted of an excitation laser source, a spectrometer and optical components including mirrors and filters. Fig. 2 shows the layout drawing of optical system with near backscattering geometry including optical cell and water chemistry loop used in this work. A more detailed description for the Raman system is given elsewhere.[29]

3. Results and Discussions

3.1. Morphology of Oxide Film on Alloy 600

Fig. 3 shows the morphology of the surface oxide film observed by a field emission scanning electron microscope (FE-SEM) for alloy 600 exposed to 350°C PWR water for 110 hours. The surface oxide film is composed of a compact layer by small crystallites of few tens of nm in diameter. Some larger crystallites of about 200 nm in diameter are present on the compact layer.

Fig. 4 shows the transmission electron micrographs of a cross-section of alloy 600 specimen oxidized in simulated PWR water with 30 cm^3(STP)/kg of dissolved hydrogen concentration for 71 hours. The thickness of oxide film on alloy 600 was observed to be in the range of 12 ~ 180 nm. Compact layers and other crystalline phases on alloy 600 observed by TEM have the same morphology as those in the FE-SEM micrographs.

3.2. Reference Raman Spectra for High Purity Oxide Powders

The first series of experiments were conducted to obtain reference Raman spectra on oxides using powder samples. Results were compared with literature data in order to verify the developed system. The results of experiments with nickel and chromium oxides and spinels in room temperature air environment are summarized in Table 2. As shown in Table 2, the Raman features of the reference powder spectra for $NiCr_2O_4$ powder show good agreements between the measurement in this work and literature data. Further details of results are given elsewhere[29].

3.3. In-situ characterization

3.3.1. Aqueous Corrosion in PWR Water with 30 cm^3(STP)/kg of Dissolved Hydrogen Concentration

To maintain the dissolved hydrogen concentration (DH_2) of 30 cm^3(STP)/kg in the

simulated PWR water, pure hydrogen gas was injected into the water storage tank with the cover gas pressure of 170 kpa. Based on Henry's law, a dissolved hydrogen concentration of 2.68 ppm is expected.[13] The operating pressure was about 18 Mpa and the temperature was gradually increased from room temperature to 350°C at an average rate of 40°C/hour. Temperatures at which Raman spectra were collected with the remained time length are summarized in Table 3.

Fig. 5 shows the in-situ Raman spectra of alloy 600 specimen obtained by holding temperatures at 250, 290, 320, and 350°C, respectively, while temperature increased. Peaks observed at ca. 417 cm^{-1}, 743 cm^{-1} in the in-situ Raman spectra were originated from the sapphire window. A feature in the range of ca. 546-587 cm^{-1} in the spectrum acquired at 250°C was known to be attributed to α-CrOOH based on Maslar et al.'s work.[19] According to the explanation described in Ref. 19, $[Cr^{III}O_6]$ octahedral are common structure to both Cr_2O_3 and α-CrOOH[21]. Therefore, one might reasonably expect the Raman wavenumbers of α-CrOOH to be observed in approximately the same wavenumber range as those of Cr_2O_3, i.e., ca. 300-613 cm^{-1}.

The crystallographic structure of the Cr_2O_3 nH_2O powder is yet unknown. The Cr_2O_3 nH_2O XRD pattern does not match any chromium hydrate/hydroxide reference patterns.[19] The broad XRD peaks are typical of a hydrate consisting of a mixture of different metastable hydrates/hydroxides. This result is consistent with a report on the Cr_2O_3 nH_2O possessing variable water content.[22] While the observed Raman peaks for Cr_2O_3 nH_2O cannot be attributed to a particular structural characteristic, the Cr_2O_3 nH_2O Raman spectrum illustrates that the Raman peaks of some hydrated Cr^{III} oxide are observed in approximately the same wavenumber range as those of Cr_2O_3. Additionally, the infrared (IR) spectrum of α-CrOOH exhibits features in this wave number range, i.e., peaks at 525 and 610 cm^{-1}.[23] Therefore, the shared structural features of Cr_2O_3 and α-CrOOH and the wavenumber range of the Raman features in the Cr_2O_3 and Cr_2O_3 nH_2O reference spectra are consistent with the assignment of the measured Raman features to α-CrOOH.

Several intense peaks are also observed in the 840-880 cm^{-1} range of spectra in Fig. 5. According to the extensive discussion by Maslar et al.[19], this feature would be attributed to Cr^{VI} or crystalline Cr^{III}/Cr^{VI} species assuming a chromium species is responsible for this feature. This explanation can account for the weak signature observed in the 340-350 cm^{-1} range in the spectra of the specimen at 250°C. Chromium oxide features in this wavenumber range are generally attributed to Cr^{VI}–oxygen terminal stretching modes or mixed Cr^{III}/Cr^{VI} oxide vibrational modes.[24] Hydrated surface chromate species have been reported to exhibit a vibrational mode at ca. 865 cm^{-1}.[25] The most intense peak in the aqueous $HCrO_4^-$ Raman spectrum is reported from ca. 880 to 899 cm^{-1}.[26,27] A number of mixed Cr^{III}/Cr^{VI} oxides have been identified during the thermal decomposition of various chromium-containing materials. Crystalline compounds such as Cr_3O_8, Cr_2O_5, and XCr_3O_8 (X = Na, K, Rb) exhibit their most intense Raman spectral features in the ca. 820-904 cm^{-1} range at room temperature. The most intense Raman spectral feature of an amorphous Cr^{III}/Cr^{VI} compound has been observed at 859 cm^{-1}. In the spectra obtained at 250 and 290 °C, weak features at 704 cm^{-1} appeared and these were attributed to nickel ferrite spinel ($NiFe_2O_4$) features.

In the spectra obtained at 320 °C, features of pure chromium oxide including α-CrOOH,

Cr^{VI} and crystalline Cr^{III}/Cr^{VI} compounds become weaker, while nickel oxide features are firstly observed and become more apparent in subsequent spectra up to 350°C. The features at 550 cm^{-1} and 910 cm^{-1} were attributed to NiO phase. Also, features of nickel chromium spinel ($NiCr_2O_4$) were detected in this temperature range. The features at ca. 682 cm^{-1} and 430 cm^{-1} were attributed to $NiCr_2O_4$ phase.[17,18] Also, nickel oxide and nickel chromite phase were still detected on the specimen surface as exposure time increases at 350 . The $NiCr_2O_4$ is one of thermodynamically stable phases in a reducing aqueous environment with the range of hydrogen overpressure at about 300°C. A more detail study that was performed to identify thermodynamically stable phase of nickel base alloy in high temperature water was described in ref. 29.

3.3.2. Aqueous Corrosion in PWR Water with 1 cm^3(STP)/kg of Dissolved Hydrogen Concentration

To maintain the dissolved hydrogen concentration of 1 cm^3(STP)/kg in water, 5% hydrogen gas balanced with 95% helium gas was injected into the water with the overpressure of 0.7 atm and it made a dissolved hydrogen concentration of 0.89 ppm in this study.[13] Temperatures at which Raman spectra were collected with the remained time length are summarized in Table 3.

Fig. 6 shows the in-situ Raman spectra of alloy 600 specimen obtained while temperature increased. A feature in ca. 546-587 cm^{-1} range in the spectrum acquired at 250°C was attributed to α-CrOOH from the dame rationale as that described earlier in the result with DH_2=30 cc/kg. Also, the intense peaks feature that would be attributed to Cr^{VI} or crystalline Cr^{III}/Cr^{VI} species was observed in the 840-880 cm^{-1} range.

As temperature increases, clear features in 550 and 910 cm^{-1} which were attributed to nickel oxide (NiO) were firstly appeared and became weaker in subsequent spectra up to 350°C. After 23 hours at 350°C in this condition, the features of nickel oxide phase were still detected on the alloy 600 specimen surface at 350 .

3.3.3. Effect of Dissolved Hydrogen Concentration Change in PWR Water

To investigate the effect of dissolved hydrogen concentration on the formation of oxide film of alloy 600 in high temperature water, dissolved hydrogen concentration was increased from 1 to 30 cc/kg, immediately following the measurement at 1 cc/kg. In-situ Raman spectroscopic measurement of alloy 600 surfaces was made both before and after the change of hydrogen concentration.

Fig. 7 shows the change of Raman spectra with the increase of dissolved hydrogen concentration in water at 350°C. In high temperature water with 1 cc/kg of hydrogen concentration, features of pure chromium oxide including α-CrOOH, Cr^{VI} and crystalline Cr^{III}/Cr^{VI} compounds and nickel oxide (NiO) features were observed at the oxide film of alloy 600 specimen. With the increase of dissolved hydrogen concentration, nickel chromium spinel ($NiCr_2O_4$) features were appeared in the observed Raman spectrum.

4. Discussion

Table 4 summarizes the comparison between experimental observations and prediction of oxide phases of alloy 600 at each condition of temperature and hydrogen concentration. It can be known that the consideration of formation of chromium oxide hydroxide (CrOOH) and nickel spinels can make differences in the thermochemical prediction results, regardless of dissolved hydrogen concentration in 350°C water. At both conditions of dissolved hydrogen concentration, nickel ferrite ($NiFe_2O_4$) phases which were predicted to be thermodynamically stable assuming that nickel spinels can be formed in this system were not experimentally detected. When the observed oxide phases are compared with the predicted stable phases of alloy 600 at 350°C, all the observed oxide phases but Cr-oxides are included in predicted stable phases. But the thermochemical predictions with CrOOH and Ni spinels do not agree with the observed results at both hydrogen concentrations in 350°C water. In contrast, the predicted Ni/NiO equilibrium line is in good agreement with the observed results. Therefore, it can be said that the oxide phases identified by in-situ Raman spectroscopic investigation can be used to verify thermodynamically stable phases.

Table 5 summarizes the experimental observations of surface oxide phases of alloy 600 in 350°C water in comparison with literature data[10,12,30] at each dissolved hydrogen concentration. At higher dissolved concentration, $NiFe_2O_4$ precipitates reported in ref. 10 and 30 could be made by Fe ion dissolution from high temperature flowing system including autoclave, tubes and fitting for longer exposure time than this thesis work. At lower dissolved concentration, the observed oxide phases agree well with those reported in literature.

From the viewpoint that electrochemical potential-pH diagrams can be useful in predicting thermodynamically stable phases, thermochemical calculations can provide very much meaningful information to explain the corrosion behavior of alloy 600 in high temperature water. Although the pH was not measured at high temperature and pressure during this investigation, this value can be estimated using aqueous thermochemical calculation softwares. In this work, pH values of primary water in PWR were calculated as a function of temperature using MULTEQ®.[28] Electrochemical potential value was calculated by using the Nernst equation assuming that the surface of alloy 600 behaves as a hydrogen electrode in the hydrogen-containing water environment. The potential of hydrogen electrode is given as below;

$$E_{H^+/H_2}(T) = E^{o}_{H^+/H_2}(T) - 2.303\,\frac{RT}{2F}\left[\log f_{H_2} + 2\,pH\right]$$
$$= -2.303\,\frac{RT}{2F}\left[\log f_{H_2} + 2\,pH\right] \quad vs.\ SHE\ (T)$$

From the results of in-situ Raman spectra of alloy 600 with temperature increase, dissolved hydrogen concentration is one of the most important experimental parameters in this study. While nickel oxide was observed at 320°C or higher at the higher hydrogen concentration, nickel oxide was observed at 290°C or higher at the lower hydrogen concentration. To compare experimental results with calculations, thermochemical calculations for alloy 600

were made as a function of temperature, as described in ref. 29. In this calculation, for simplicity, it was assumed that nickel oxide could be produced whereas spinel oxide could not form. In Fig. 8, dashed line represents a previous experimental result of nickel/nickel oxide transition using a contact electric resistance (CER) instrument.[31] The deviation between present and previous study can arise from inaccuracy of thermochemical data at high temperature for calculation in this work or experimental uncertainty in previous work.

Fig. 8 summarizes the estimated electrochemical potential of alloy 600 for two different hydrogen concentrations in this experiment as a function of temperature. It can be seen that nickel oxide was in a thermodynamically stable state at 270°C or higher at the lower hydrogen concentration. NiO phase was observed to be stable at 320°C or higher at the higher hydrogen concentration.

In-situ Raman spectroscopy is shown to be a very useful experimental tool that can provide valuable information about oxide films and the SCC behavior of alloy 600 in high temperature aqueous environments. In this work, dissolved hydrogen concentration was experimentally known to play an important role on the formation of oxide films on the alloy 600 in high temperature water. Different compositions of oxides were produced at different condition of dissolved hydrogen concentration in high temperature water.

Previous studies showed that the dissolved hydrogen concentration of 30 cm^3(STP)/kg at 360°C corresponded to the maximum susceptibility of alloy 600 to crack initiation. The present in-situ Raman spectroscopic study showed that the condition corresponds to Ni/NiO equilibrium line in agreement with thermochemical predictions. Based on the results, it can be concluded that the mixture of nickel and chromium spinel oxide on the surface of alloy 600 is more sensitive to the SCC initiation than nickel oxide on that in 350°C PWR water condition. Mechanistic understanding on why the condition leads to the higher susceptibility to SCC of alloy 600 in PWR water may require a more detailed study on the nanostructure of oxide films that is beyond the scope of this study.

5. Summary and Conclusion

In-situ Raman spectroscopic investigation has been conducted for a nickel-base alloy 600 exposed to deaerated water with 1,000 ppm boron and 2 ppm lithium at a pressure of 18 Mpa, temperatures ranging up to 350°C and dissolved hydrogen concentrations ranging from 1 to 30 cc/kg in an optically accessible cell. From this study, following conclusions are made:

1. An in-situ Raman spectroscopic system was developed successfully to provide valuable information for the oxide film of structural alloys in water reactor environments, as a function of temperature, water chemistry and stress.

2. Potential-pH diagrams for Ni-Cr-Fe alloy at high temperature water were predicted by thermochemical calculations considering both ternary alloying effect and spinel oxide formation.

3. At the lower dissolved hydrogen concentration (1 cm^3(STP)/kg), nickel oxide(NiO) phase was detected on the specimen surface at temperature ranges between 290 and 350 . Nickel oxide phase appeared to be stable over a long period of time (21 hours) at 350 .

4. At the higher dissolved hydrogen concentration (30 cm^3(STP)/kg), chromium oxide

hydroxide (CrOOH) phase was detected on the specimen surface at relatively low temperature ranging from 250 to 290 . Also, features attributed to the phase of NiO and $NiCr_2O_4$ were observed at 320 or higher.

5. Thermochemical calculations on the formation of NiO agreed very well with the in-situ Raman observation results.

6. Irrespective of dissolved hydrogen concentration, CrOOH, $Ni(Fe)Cr_2O_4$, and $NiFe_2O_4$ were predicted to be stable in 350℃ water, assuming the formation of nickel spinels. CrOOH, NiO and $FeCr_2O_4$ were predicted to be stable in 350℃ water, assuming the absence of nickel spinels.

7. Based on the results of in-situ Raman spectroscopic measurement and thermochemical calculation of oxide film on alloy 600, the mixture of nickel and chromium spinel oxide on the surface of alloy 600 is more sensitive to the SCC initiation than nickel oxide on that in 350℃ PWR water condition.

Acknowledgements

The authors would like to express their gratitude to Dr. J. Maslar and Dr. W. Hurst of the National Institute of Standards and Technology, Gaithersburg, MD, USA. Professor Y.W. Kim of Seoul National University kindly helped electron microscope examinations. This work was supported by the National Nuclear R&D programs of the Korean Ministry of Science and Technology.

References

1. J.M Gras, “Stress corrosion cracking of steam generator tubing materials - review and assessment”, Parkins Symposium on Fundamentals Aspects of Stress Corrosion Cracking, TMS, 1992, p. 411.

2. T.M. Angeliu, P.L. Andresen and F.P. Ford, “Applying slip-oxidation to the SCC of austenitic materials in BWR/PWR environments”, Corrosion 98, NACE (1998), Paper No. 262.

3. T. Magnin, J-M. Boursier, D. Noel, R. Rios, and F. Vaillant, “Corrosion-deformation interaction during stress corrosion cracking of alloy 600 in primary water”, Proceedings of the 6th International Symposium on Environmental Degradation of Materials in Nuclear Power System – Water Reactors, TMS, 1993, p.669.

4. P.M. Scott and M. Le Calvar, “Some possible mechanisms of intergranular stress corrosion cracking of alloy 600 in primary water”, Proceedings of the 6th International Symposium on Environmental Degradation of Materials in Nuclear Power System – Water Reactors, TMS, 1993, p. 657.

5. P.M. Scott, “An Overview of internal oxidation as a possible explanation of intergranular stress corrosion cracking of alloy 600 in PWRs”, Proceedings of the 9th International Symposium on Environmental Degradation of Materials in Nuclear Power System – Water Reactors, TMS, 1999, p. 3.

6. G. Was, T.M. Angeliu, and J.K. Sung, “Deformation and intergranular cracking behavior of Ni-Cr-Fe alloys at high temperature”, Proceedings of the “Specialist Meeting on Environmental Degradation of Alloy600”, Airlie House, VA, April 1993, EPRI Report TR-104898, 1996, p. 24-1.

7. M.M. Hall, “Thermally activated low temperature creep and primary water stress corrosion cracking of NiCrFe alloys”, Proceedings of the “Specialist Meeting on Environmental Degradation of Alloy600”, Airlie House, VA, April 1993, EPRI Report TR-104898, 1996, p. 6-1.

8. R.S. Pathania, and A.R. Mcilree, “A review of the effect of hydrogen on stress corrosion cracking of alloy 600 in 360℃ water”, Proceedings of the 3rd International Symposium on Environmental Degradation of Materials in Nuclear Power System – Water Reactors, AIME, 1987, p. 551.

9. T. Cassagne and A. Gelpi, “Crack growth rate measurements an alloy 600 steam generator tubing in primary and hydrogenated AVT water”, Proceedings of the 8th International Symposium on Environmental Degradation of Materials in Nuclear Power System – Water Reactors, TMS, 1993, p.679.

10. C. Soustelle, M. Foucault and P. Combrade, “PWSCC of alloy 600: a parametric study of surface film effects”, Proceedings of the 9th International Symposium on Environmental Degradation of Materials in Nuclear Power System – Water Reactors, TMS, 1999, p. 105.

11. T. Cassagne, B. Fleury, O. De Bouvier, and P. Combrade, “An Update of the Influence of Hydrogen on the PWSCC of nickel base alloy in high temperature water”, Proceedings of the 8th International Symposium on Environmental Degradation of Materials in Nuclear Power System – Water Reactors, TMS, 1997, vol. 1, p. 307.

12. D. Caron, PhD. Thesis, INSA-Lyon Scientific and Technical University, France, 2000.

13. D.M. Himmelblau, “Solubilities of inert gases in water 0℃ to near the critical point of water”, J. Chem. Eng. Data 5 1 (1960) 10.

14. W.S. Hurst, M.S. Hodes, W.J. Bowers Jr., V.E. Bean, J.E. Maslar, and K.A. Smith, “Optical flow cell and apparatus for solubility, salt deposition and Raman spectroscopic studies in aqueous solutions near the water critical point”, Journal of Supercritical Fluids 22 (2002) 151.

15. J.E. Maslar, W.S. Hurst, W.J. Bowers Jr., J.H. Hendricks, and M.I. Aquino, “In situ Raman spectroscopic investigation of nickel hydrothermal corrosion”, Corrosion 58 (2002) 225.

16. R.E. Dietz, G.I. Parisot, and A.E. Meixner, “Infrared Absorption and Raman Scattering by Two-Magnon Processes in NiO”, Phys. Rev. B, Condens. Matter 4 (1971) 2302.

17. J.E. Maslar, W.S. Hurst, W.J. Bowers Jr., and J.H. Hendricks, “In situ Raman spectroscopic investigation of stainless steel hydrothermal corrosion”, Corrosion 58 (2002) 739.

18. M.D. Cunha Belo et al., “Composition, structure and properties of the oxide films formed on the stainless steels 316L in a primary type PWR environment”, Corrosion Science 40 23 (1998) 447.

19. J.E. Maslar, W.S. Hurst, W.J. Bowers Jr., J.H. Hendricks, M.I. Aquino and I. Levin, “In situ Raman spectroscopic investigation of chromium surface under hydrothermal conditions”, Applied Surface Science 180 (2001) 102.

20. R.L. Mccreery, “Raman spectroscopy for chemical analysis”, Wiley-Interscience, 2000.

21. A.F. Well, “Structural inorganic chemistry”, 5th edition, Clarendon Press, Oxford, 1984.

22. F.A. Cotton, and G. Wilkinson, “Advanced inorganic chemistry: A comprehensive test”, 5th edition, Wiley, New York, 1980.

23. R.G. Snyder, and J.A. Ibers, “O-H-O and O-D-O potential energy curves for chromous acid”, J. Chem. Phys. 36 (1962) 1356.

24. J.E. Maslar, W.S Hurst, T.A. Vanderah and I. Levin, “The Raman spectra of Cr_3O_8 and Cr_2O_5”, J. Raman Spectrosc. 32 (2001) 201.

25. B.M. Weckhuysen, I.E. Wachs and R.A. Schoonheydt, “Surface chemistry and spectroscopy of chromium in inorganic oxides”, Chem. Rev. 96 (1996) 3327.

26. J.B.B. Heyns, J.J. Cruywagen and K.T. Carron, “Raman spectroscopic investigation of chromium (VI) equilibrium-another look”, J. Raman Spectrosc. 30 (1999) 335.

27. G. Michel and R. Machiroux, “Raman spectroscopic investigation of the $Cr_2O_4^{2-}$ /$Cr_2O_{47}^{2-}$ equilibrium in aqueous solution”, J. Raman Spectrosc. 14 (1983) 22.

28. “MULTEQ: Equilibrium of an electrolytic solution with vapor-liquid partitioning, Volume 3: Theory manual”, EPRI NP-5561-CCML, Volume 3, EPRI, Palo Alto, CA, 1992.

29. J.H. Kim, Ph. D. Dissertation, Seoul National University, Republic of Korea (2003)

30. T. Terachi et al., “Characterization of oxide film on alloy 600 in PWR primary water,” Proceedings of Join Meeting of EAC-A, EAC-J and CUP on Environmentally Assisted Cracking of Water Reactor Materials, Tohoku Univ., Japan (2002).

31. S.A. Attanasio, D.S. Morton, M.A. Ando, N.F. Panayotou and C.D. Thompson, “Measurement of the nickel/nickel oxide phase transition in high temperature hydrogenated water using the contact electric resistance (CER) techniques”, Proceedings of the 10th International Symposium on Environmental Degradation of Materials in Nuclear Power System – Water Reactors, NACE, 2001.

Table 1. Chemical Composition of Alloy 600 Used in This Study (wt.%)

Element	C	Mn	Fe	S	Si	Cu	Ni	Cr	Al	Ti	Nb	P	B	N
Compo.	0.06	0.26	8.31	0.001	0.3	0.12	75.12	15.25	0.16	0.36	0.04	0.09	0.02	0.01

Table 2. Nominal Raman Peak Wavenumbers for Oxide Powders[a] Measured in Room Temperature Air Environment.

Oxide	This work[b]	Ref. 1[c]	Ref. 2[c]
NiO	1,074	1,074 [15]	
	910	913 [15]	
	725	727 [15]	
	532	535 [15]	490 [15]
	400	370 [15]	
$NiFe_2O_4$	702	705 [17]	700 [18]
	654[sh]	655 [17]	655 [18]
	595	592 [17]	
	574	570 [17]	579 [18]
	492	488 [17]	490 [18]
	460	457 [17]	433 [18]
Cr_2O_3	610	613 [19]	585 [19]
	550	552 [19]	554 [19]
	528	527 [19]	488 [19]
	352	350 [19]	387 [19]
	302	300 [19]	352 [19]
$NiCr_2O_4$	687	685 [17]	686 [18]
		616 [17]	
		585 [17]	
	550-560	554 [17]	
	513	514 [17]	512 [18]
	429	430 [17]	

[a] The most intense peak(s) in each spectrum is underlined.
[b] The wavenumber of a well-resolved peak has an associated uncertainty of ±2 cm^{-1}.
[c] The excitation laser with 647.1nm wavelength was used.

Table 3. Temperature and Exposure Time of Alloy 600 Specimen Prior to In-Situ Raman Spectra Measurements in High Temperature Water.

DH2 (cc/kg)	Temperature (°C)	Total exposure time prior to first measurement at temperature (h)	Hold time at each temperature prior to first measurement (h)
30	250	28	2
	290	33.5	3
	320	42	7
	350-I	47.5	3.5
	350-II	69.5	20.5
1	250	40	33
	290	45	3
	320	48	2
	350-I	51	2
	350-II	74	23

Table 4. Summary of Experimental Observations and Thermochemical Predictions of Surface Oxide Phases of Alloy 600 in 350°C Water at Each Dissolved Hydrogen Concentration.

	Predicted at 350 °C			Observed at 350 °C
		With Ni spinels	Without Ni spinels	
DH_2 = 30cc/kg	With CrOOH	CrOOH $NiFe_2O_4$	CrOOH NiO	NiO $NiCr_2O_4$ CrOOH Cr-Oxide
	Without CrOOH	$NiCr_2O_4$ $FeCr_2O_4$	NiO $FeCr_2O_4$	
DH_2 = 1cc/kg	With CrOOH	CrOOH $NiFe_2O_4$	CrOOH NiO	NiO CrOOH Cr-Oxide
	Without CrOOH	$NiCr_2O_4$ $FeCr_2O_4$	NiO $FeCr_2O_4$	

Table 5. Summary of Experimental Observations of Surface Oxide Phases Of Alloy 600 in 350°C Water in Comparison with Literature Data at Each Dissolved Hydrogen Concentration.

	This work	Soustelle[11]	Caron[12]	Terachi[30]
Method	In-situ Raman	GDOS + EDS	XPS	Synchrotron XRD + TEM
Temperature (°C)	350	360	330	320
Exposure time (hrs)	70	300	1869	1000
Oxide(s) at high DH_2	CrOOH, Cr-Oxide NiO+$NiCr_2O_4$	Compact layer ($NiCr_2O_4$)+ Precipitates ($NiFe_2O_4$)	$NiCr_2O_4$	(Ni+Cr-rich) oxide + Precipitates ($NiFe_2O_4$)
Oxide(s) at low DH_2	CrOOH, Cr-Oxide NiO	Compact layer ($NiCr_2O_4$)	NiO	NiO

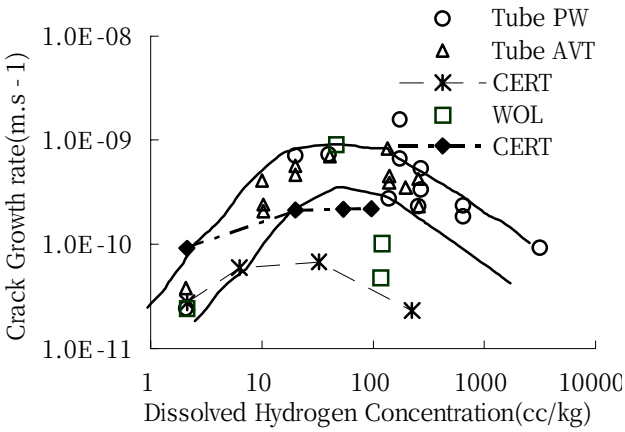

Fig. 1 Influence of hydrogen concentration on the crack growth rate of PWSCC in alloy 600 at 360℃.[10]

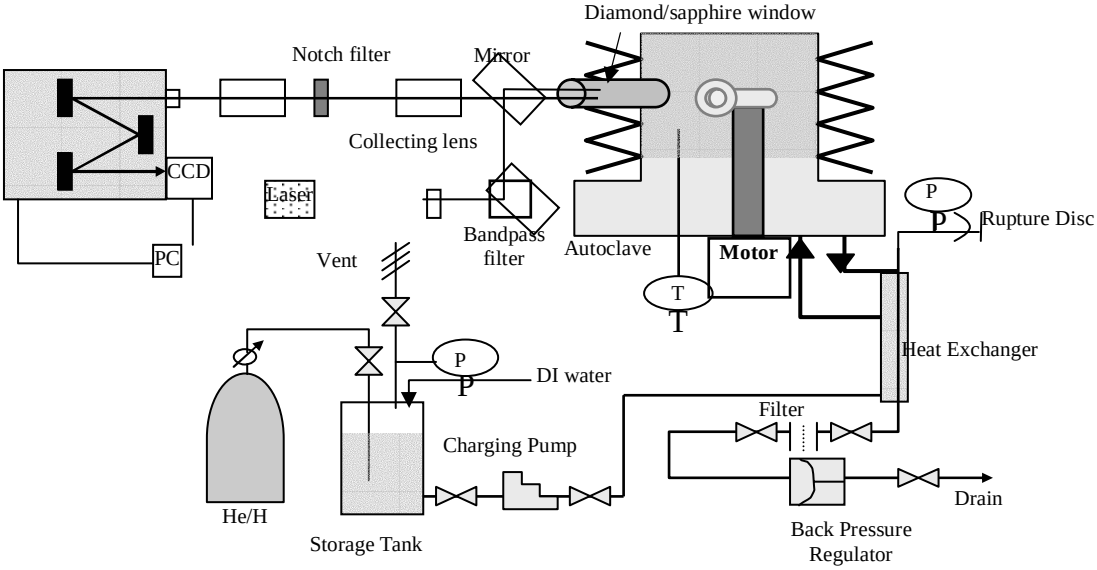

Fig. 2 Layout of in-situ Raman spectroscopic measurement system in high temperature aqueous environment.

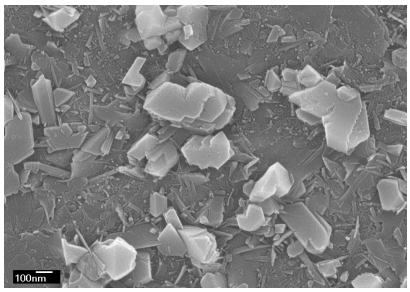

Fig. 3 Field emission scanning electron micrographs of oxide film on alloy 600 after 110 hours exposure in simulated PWR water.

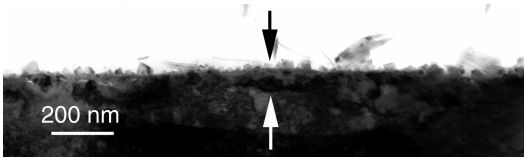

Fig. 4 TEM micrographs of oxide film on alloy 600 after 71 hours exposure in simulated PWR water.

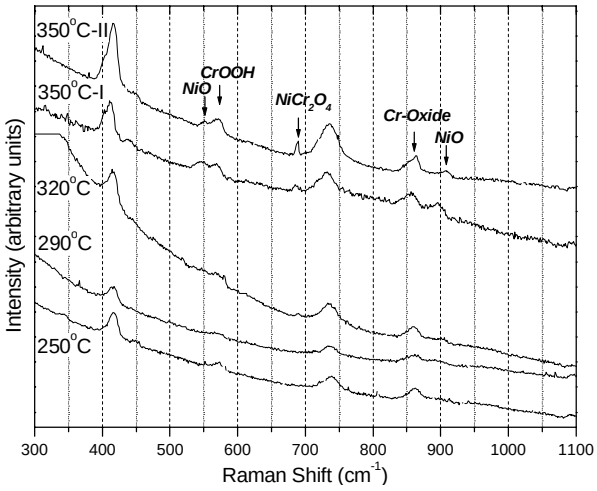

Fig. 5 In-situ Raman spectra obtained for alloy 600 by holding at 250, 290, 320 and 350℃, respectively, during heating up to 350 ℃ in PWR water condition with DH_2=30cc(STP)/kg.

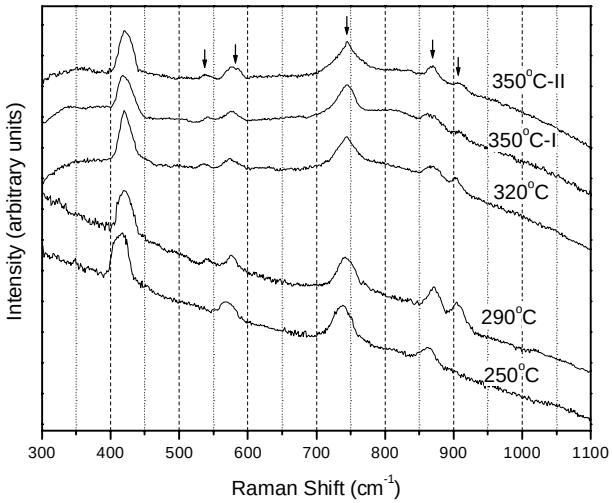

Fig. 6 In-situ Raman spectra obtained for alloy 600 by holding at 250, 290, 320 and 350℃, respectively, during heating up to 350℃ in PWR water condition with DH_2=1cc(STP)/kg.

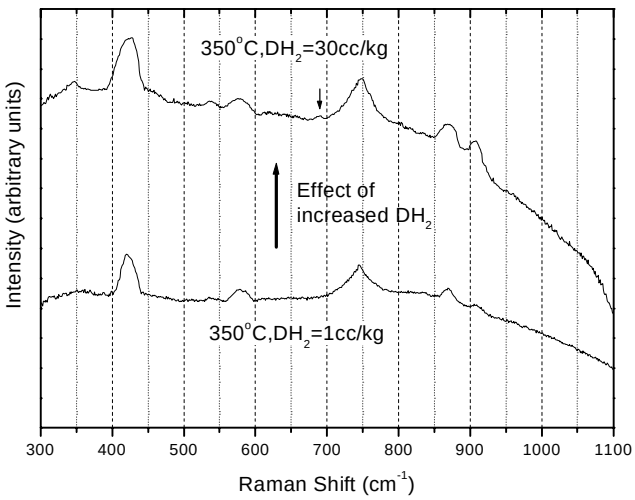

Fig. 7 In-situ Raman spectra obtained for alloy 600 at 350℃ in PWR water as the DH_2 in water was increased from 1 to 30 cc/kg.

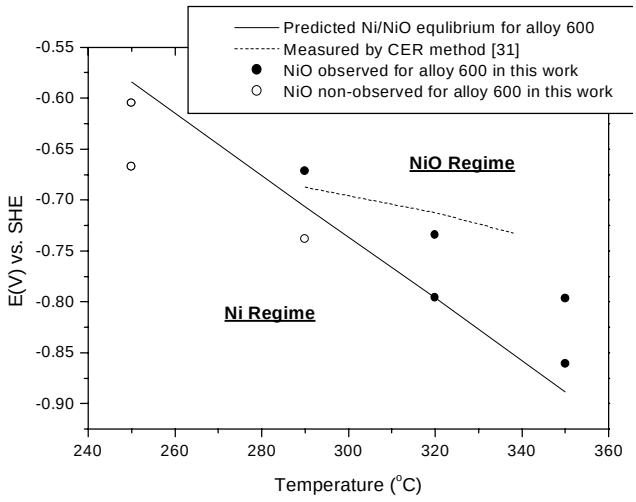

Fig. 8 Summary plot on electrochemical potential for nickel in the alloy 600 as a function of temperature.